

Inkjet-printed bipolar resistive switching device based on Ag/ZnO/Au structure

Cite as: Appl. Phys. Lett. **119**, 112103 (2021); <https://doi.org/10.1063/5.0058526>

Submitted: 31 May 2021 • Accepted: 22 August 2021 • Published Online: 15 September 2021

 Hongrong Hu, Alexander Scholz,  Surya Abhishek Singaraju, et al.



View Online



Export Citation



CrossMark

ARTICLES YOU MAY BE INTERESTED IN

[A comprehensive review on emerging artificial neuromorphic devices](#)

Applied Physics Reviews **7**, 011312 (2020); <https://doi.org/10.1063/1.5118217>

[Aqueous solution-deposited aluminum-gallium-oxide alloy gate dielectrics for low voltage fully oxide thin film transistors](#)

Applied Physics Letters **119**, 112102 (2021); <https://doi.org/10.1063/5.0057806>

[Reliability of analog resistive switching memory for neuromorphic computing](#)

Applied Physics Reviews **7**, 011301 (2020); <https://doi.org/10.1063/1.5124915>

 **Lake Shore**
CRYOTRONICS



240 Series Sensor Input Modules

For precision cryogenic temperature monitoring over PLC networks [LEARN MORE](#) 

Inkjet-printed bipolar resistive switching device based on Ag/ZnO/Au structure

Cite as: Appl. Phys. Lett. **119**, 112103 (2021); doi: [10.1063/5.0058526](https://doi.org/10.1063/5.0058526)

Submitted: 31 May 2021 · Accepted: 22 August 2021 ·

Published Online: 15 September 2021



View Online



Export Citation



CrossMark

Hongrong Hu,¹ Alexander Scholz,^{1,2} Surya Abhishek Singaraju,¹ Yushu Tang,¹ Gabriel Cadilha Marques,¹ and Jasmin Aghassi-Hagmann^{1,2,a)}

AFFILIATIONS

¹Institute of Nanotechnology, Karlsruhe Institute of Technology, Hermann-von-Helmholtz-Platz 1, 76344 Eggenstein-Leopoldshafen, Germany

²Institute for Applied Research, Offenburg University of Applied Sciences, Badstraße 24, 77652 Offenburg, Germany

^{a)}Author to whom correspondence should be addressed: jasmin.aghassi@kit.edu

ABSTRACT

In this Letter, we report an inkjet-printed resistive switching device based on an Ag/ZnO/Au structure. The device exhibits bipolar resistive switching behavior, a low operation voltage of about 0.7 V, a high on/off ratio of 10^7 , a long retention time exceeding 10^4 s, and good endurance. The conduction mechanism of the device in low and high resistive states was studied and showed good consistency with the theory of Ohmic and space charge limited conduction mechanisms, respectively.

Published under an exclusive license by AIP Publishing. <https://doi.org/10.1063/5.0058526>

Resistive switching (RS) in various classes of materials and corresponding devices, also referred to as memristive devices and memristors,^{1–4} allows for new data storage solutions,^{5,6} and can be used to empower novel paradigms in computing such as beyond-von-Neumann architectures and neural networks.^{7,8} Metal oxide-based memristors show promising features such as high device on-/off ratios, complementary metal-oxide-semiconductor (CMOS) fabrication compatibility,⁹ and solution processability.¹⁰ With an increasing demand in printed electronics-based devices and systems, possibilities for lightweight data storage are required, which can be tackled using printed memristors. Solution processed resistive switching devices with good memory performance have been reported, for instance, fabricated by spin coating.^{11,12} In addition, the potential of solution processed memristors in computing is explored by Lu *et al.*¹³ The attempt to mimic the plasticity of biological synapses through a fully printed memristive device is reported by Feng *et al.*¹⁴ Nelo *et al.* investigated inkjet-printed copper oxide and titanium oxide, obtained from precursors as storage layers, in memristive devices.¹⁵ However, the presented devices exhibit low on-/off ratios. Furthermore, memristive behavior was also found in inkjet-printed graphene oxide layers.¹⁶ Among various possible materials for the storage layer of memristors, metal oxides gained the most interest from academia due to its wide range of electrical properties.¹⁷ In the group of metal oxides, zinc oxide (ZnO) is of interest since it is a biocompatible, environmentally friendly semiconductor with a wide bandgap of 3.3 eV. Furthermore, it offers high

transparency, excellent chemical stability, high carrier mobility, and a low price.^{17–19} In this work, we introduce inkjet-printed memristors incorporating poly-crystalline hexagonite wurtzite zinc oxide as a memristor storage layer material, which is sandwiched between an inkjet-printed silver top electrode and a gold bottom electrode. The device shows high electrical performance such as high on-/off switching ratios of $\approx 10^7$ and good endurance and retention times. The inkjet-printed zinc oxide storage layer is investigated using x-ray powder diffraction (XRD) and scanning electron microscopy (SEM) to reveal information about the layer quality and its overall structural properties.

The fabrication process of the resistive switching device in this work is described in the following. A layer of gold, with a thickness of 45 nm, is deposited on a chromium-covered glass substrate by thermal evaporation (Leybold systems, Univex 350G). The 5 nm thick chromium seed layer is thermally evaporated on a glass substrate in order to provide good adhesion of the following gold film. Structuring of the gold bottom electrode is achieved by laser ablation, using a Trumpf TruMicro 5000 ps laser, which is operated with an average power of 1.5 W. The storage layer, covering the gold electrode, is fabricated by inkjet printing of an in-house prepared, zinc nitrate-based salt precursor fluid [$0.1 \text{ M Zn}(\text{NO}_3)_2 \cdot 6\text{H}_2\text{O}$] with a drop-on-demand piezo inkjet-printer (DMP2831, Fujifilm), which is an established route for inkjet-printed, thin-film device fabrication.²⁰ After printing, annealing of the precursor at 400°C over 2 h is required to form the ZnO

thin-film. For the top electrode, a commercially obtained silver nanoparticle ink (Silverjet DGP, Sigma Aldrich) was inkjet-printed onto the ZnO layer vertically to build a crossing junction with the bottom electrode and subsequently annealed at 150 °C for 1 h. Figure 1(a) displays the layout of the Ag/ZnO/Au memristor from the top view. The size of the effective resistive switching (RS) area, also labeled as the junction area, depends on the width of the top and bottom electrodes, which forms the crossing junction of the sandwiched ZnO storage layer. The inkjet-printed memristor junction area is $\approx 50 \times 50 \mu\text{m}^2$ for our fabricated devices, as shown in the microscopic image on the right-hand side of Fig. 1(a). The vertical structure of the inkjet-printed device is schematically and optically illustrated in Fig. 1(b) using scanning electron microscopy (SEM) (FEI strata 400 S). The thickness of the material stack can be determined, as Ag ≈ 80 nm, ZnO ≈ 200 nm, and Au ≈ 45 nm. For the ZnO crystal structure and chemical composition analysis, XRD analysis (Bruker D8 Advance Powder Diffractometer) is performed. It reveals a clear transformation to zinc oxide from the zinc

nitrate-based, inkjet-printed precursor. The XRD results are shown in Fig. 1(c) and no observable peaks, except for ZnO, are visible. The storage layer is formed in a poly-crystalline hexagonal wurtzite ZnO structure (compared with JCPDS card 36-1451).

In the following, electrical characterization of the inkjet-printed devices is performed. All electrical measurements are conducted on a probe station (MPS150, Cascade) at room temperature and with a semiconductor parameter analyzer (4200A SCS, Keithley). The resistive switching (RS) behavior of the memristors developed in this work is primarily investigated by current-voltage (I - V) analysis, as visualized in Fig. 2(a). The sweeping voltage measurement was executed at a fixed sweeping rate of 0.01 V/step. For the set process, which switches the device from the high resistive state (HRS) to the low resistive state (LRS), the voltage was swept from 0 to 1.5 V and back to 0 V. For the reset process, in order to switch the device from the LRS to the HRS, the voltage was swept from 0 to -1.2 V and back to 0 V. To prevent the device under test from breakdown, a compliance current (CC) of 0.8 mA was chosen to limit the maximum current during the set

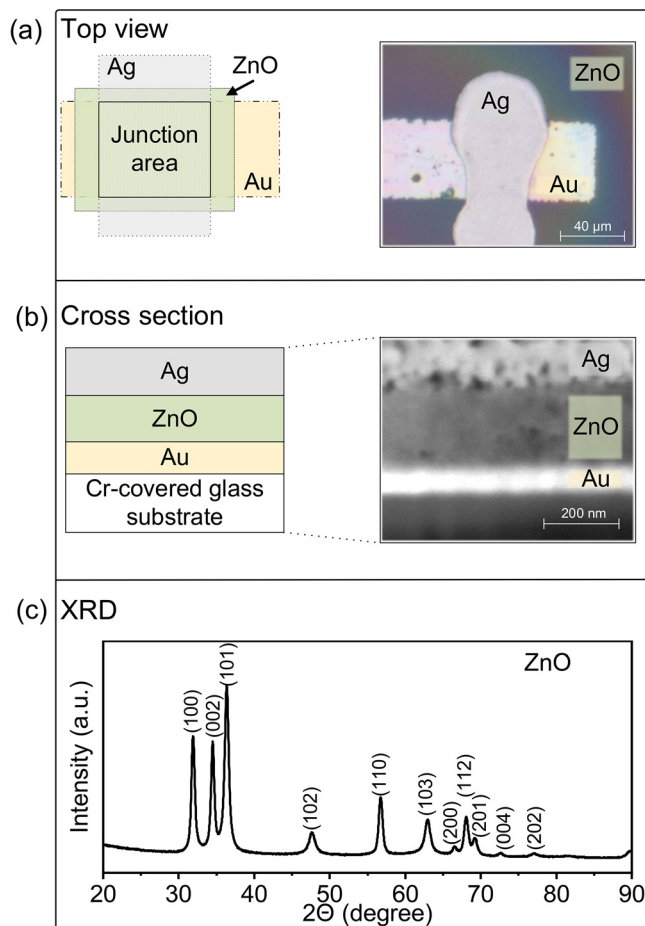


FIG. 1. (a) Schematic top section and a microscopic image of the Ag/ZnO/Au memristor is shown. (b) Schematic cross section, which shows the device stack and a corresponding SEM cross-sectional image. (c) XRD patterns of the inkjet-printed ZnO, which was transformed from zinc nitrate-based precursor salt.

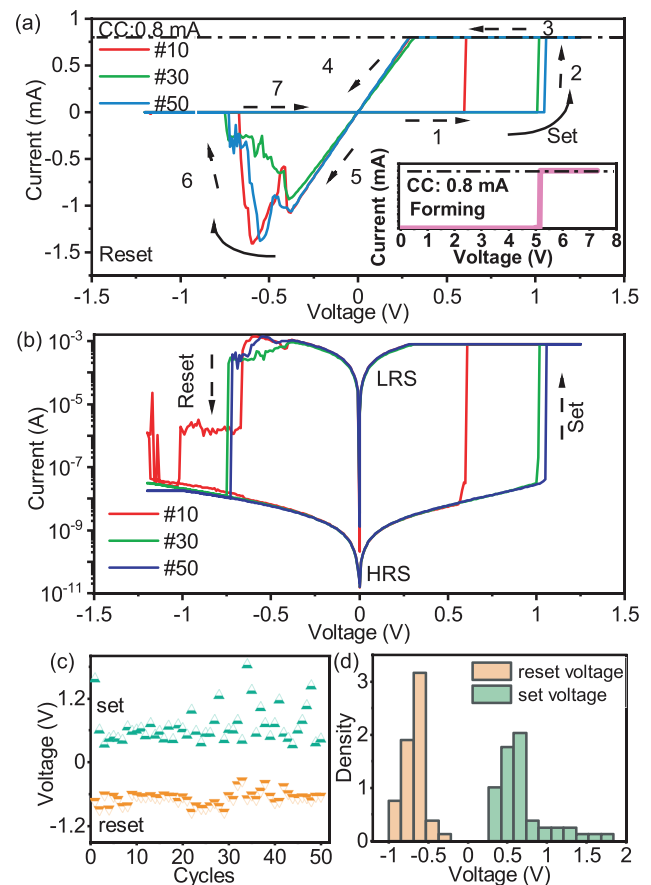


FIG. 2. (a) Bipolar I - V curves on a linear scale. The dashed arrows and labeled numbers depict the sequence of the sweeping voltage. The solid, curved arrows show the resistive switching moment. For the set process, a compliance current of 0.8 mA is used. The small inset highlights the device forming process. (b) I - V curves plotted on a semilogarithmic scale. (c) Set and reset voltage evolution of a single device within 50 RS cycles. (d) Set and reset voltage distribution of a single device within 50 RS cycles.

process. This value was selected after multiple experiments to ensure the best RS performance, since the level of the CC could have an impact on RS during the electrical measurements. This phenomenon was also observed and studied in the literature.^{21,22} The bias voltage was applied to the top electrode throughout I - V characterization, while the bottom electrode was grounded. A typical bipolar resistive switching behavior can be observed from the obtained curves, since the set and reset processes were completed at opposite voltage polarities. In addition, the I - V curves reveal that the RS mechanism of the investigated device is based on an electrochemical mechanism (ECM), as shown by Zhang *et al.*²³ The small inset in Fig. 2(a) depicts that the forming process is completed at about 5 V, which is described as the first RS for a fresh device from initial HRS to LRS. For the set process, an abrupt increase in the current can be observed at 0.5 V for the tenth loop and at around 1 V for 13th and 15th loop, which indicates a transformation from the HRS to the LRS of the device under test. The voltage, at which the RS happens, is labeled as the set voltage. The reduced set voltage of the tenth loop may be due to a small amount of conductive filament forming at the beginning. For the reset process, the device was switched back to HRS at around -0.7 V. The peak-like curves of the reset process indicate multiple conductive filaments, which cannot be ruptured at once. To reveal more detail of the resistive switching, the I - V characteristics are plotted on a semilogarithmic scale in Fig. 2(b). During RS, the curves exhibit steep slopes, which represent rapid set and reset processes. An outstanding cycle-to-cycle homogeneity of set/reset voltages of the individual device is presented in Figs. 2(c) and 2(d) by plotting the evolution and distribution of the set and reset voltages within 50 RS cycles. It is worth noting that the device is ready to be set at around 0.7 V and to be reset at around -0.7 V [see Fig. 2(d)], which is extremely competitive for the low operation voltage among reported solution processed metal oxide resistive switching devices.²⁴

To investigate the device-to-device variation of the operation voltage of inkjet-printed memristors, the forming, set, and reset voltages of 40 devices were measured and visualized as histograms in Fig. 3. Although the voltage to enable the first resistive switching in a fresh memristor is difficult to forecast accurately, for most devices in our case, it varies between 1.5 and 7 V [see Fig. 3(a)], the set and reset voltages present an excellent consistency, once the conductive filaments exist steadily in the ZnO layer. The set and reset voltages are distributed mainly around 1.6 V [see Fig. 3(b)] and -0.9 V [see Fig. 3(c)], respectively.

The switching endurance of the inkjet-printed memristor was investigated under the pulsed voltage mode, and the device was switched between the HRS and the LRS in over 500 cycles. The

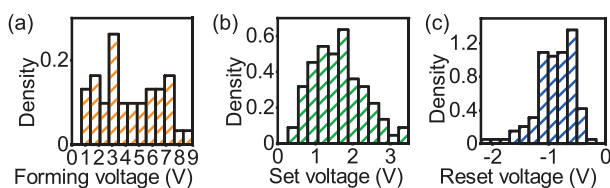


FIG. 3. Device-to-device variation of the operation voltage is depicted by plotting histograms of (a) forming, (b) set, and (c) reset voltages. Data are collected from 40 devices.

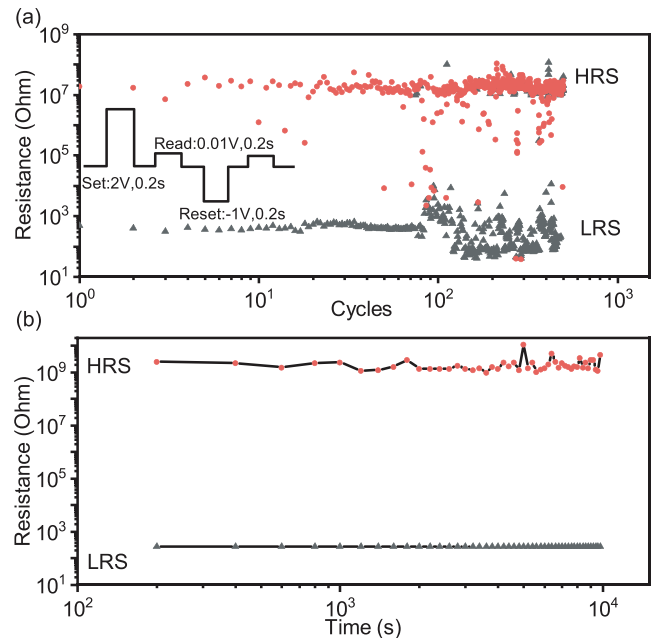


FIG. 4. (a) The resistive switching endurance of the studied memristor under the short pulse voltage mode within 500 cycles. The small inset in (a) exhibits the voltage waveform of pulse endurance measurement. (b) The stable retention performance of both resistive states within 10^4 s.

resistance values of HRS and LRS are plotted in Fig. 4(a). For a resistive state readout of the device under test, a readout voltage of 0.01 V, which is too low to affect the conductive filaments, was employed after each RS operation. Under the pulse voltage mode [for results, see Fig. 4(a)], a set pulse of 2 V is applied over a duration of 0.2 s, and the reset pulse of -1 V was also applied with a duration of 0.2 s. Both voltages were applied for stimulating the device sequentially, and each voltage stimulation is followed by a resistance read pulse voltage. The corresponding waveform is shown in the small inset of Fig. 4(a) and was executed automatically by the semiconductor analyzer. As Fig. 4(a) shows, within the first 100 cycles, the device can be switched reliably between the HRS and the LRS with a high on/off ratio exceeding 10^4 . (The HRS possesses resistance of about $10^7 \Omega$ while the LRS exhibits resistance smaller than $10^3 \Omega$.) After 100 switching cycles, the device is apt to broaden the window between two resistive states by shrinking resistance in the LRS. As a side effect, the resistive state of the device cannot be fully switched by pulse stimuli. This phenomenon may be due to the increasing of conduction filaments during the continuous switching operations. However, it is worth noting that there is no obvious degradation of two resistive states after 500 switching cycles under pulse testing modes. This highlights a high reliability of the inkjet-printed device for memory applications.

The retention of the device in this work was also studied and is presented in Fig. 4(b). There is no obvious tendency that the resistances of both resistive states are getting close to each other within 10^4 s. No indication of degradation appears at the end of the retention test. The excellent retention performance enables the device to be a promising candidate as nonvolatile memory. Aside from that, the very high on/off-ratio of 10^7 could be achieved with around $10^9 \Omega$ for HRS and

$10^2 \Omega$ for LRS for the device employed in the retention test, which could be comparable to the performance of devices fabricated by high quality processes such as plasma enhanced atomic layer deposition.²⁵

The key performance parameters of inkjet-printed memristors reported in this work and in other published works are listed in Table I. Compared with inkjet-printed memristors based on other reported structures, the device comprising Ag, ZnO, and Au, which is presented in our work, exhibits excellent reliability due to a long retention time of 10^4 s and a good endurance of 500 resistive switching cycles.

In the following, we explore and explain the conducting mechanism in more detail. To investigate the conducting mechanism during an applied voltage to the device, the I - V curves of set and reset processes are, respectively, plotted on a double logarithmic scale in Figs. 5(a) and 5(b). A linear fit over the I - V curves over different resistive states and various voltage regions was done to obtain the slope of the curve, which can be a feasible approach to reveal the conduction mechanism.³⁰ The I - V characteristics of the LRS, both in the set and reset processes, are in good agreement with Ohmic conduction and a slope of about 1.00 in accordance with Chiu.³⁰ In addition, the high current level of the LRS is contributed to the high conductivity, which indicates the formation of silver conducting filaments in the ZnO layer. The conduction mechanism of the LRS is illustrated by a schematic on the left side of Fig. 5(c). In contrast to the LRS, governed by a single mechanism, the fitting results of the HRS with multiple slope values can be linked to trap-controlled space charge limited conduction (TC-SCLC).³¹ The conduction behavior of the HRS occurs at the ZnO gap between the tip of the ruptured silver filament and the silver electrode [as shown in the right side of Fig. 5(c)]; therefore, the conduction mechanisms in this case are more complicated and need to be discussed within different voltage regions. For the low voltage region, in the set process, the I - V curves fit Ohm's law, as the slope of the fitting line is around 1.06. For this low field regime, the current can be attributed to the minuscule amount of the thermally excited charge carriers in the active layer;³² consequently, an extremely small magnitude of current compared with that of the LRS can be observed in Fig. 5(a). As the applied voltage increases, the electrons from the metallic electrode can be injected into the ZnO layer and partially fill traps, which leads to a slight growth of the conductance, showing a larger slope of 1.77. This I - V relationship is classified to trap-unfilled space charge limited conduction (SCLC), obeying Child's square law with $I \propto V^2$, as discussed by Zhu *et al.*³³ As the external electrical field is further increased, the electrons originating from the electrode filled up the

TABLE I. Performance comparison between our work and other reported memristors fabricated by inkjet printing.

Structure	$R_{on/off}$ ^a	Retention (s)	Endurance (cycles)	Reference
ITO/ZnSnO ₃ /Ag	10	1.2×10^4	2×10^2	26
Ag/HfO ₂ /Au	10^3	n.d. ^b	1.28×10^2	27
Ag/ZrO ₂ /Ag	10^2	n.d.	1.4×10^2	28
Cu/CuO/AgO/Ag	10	n.d.	4×10^1	29
Ag/ZnO/Au	10^7	10^4	5×10^2	This work

^aResistance on/off ratio.

^bNot defined.

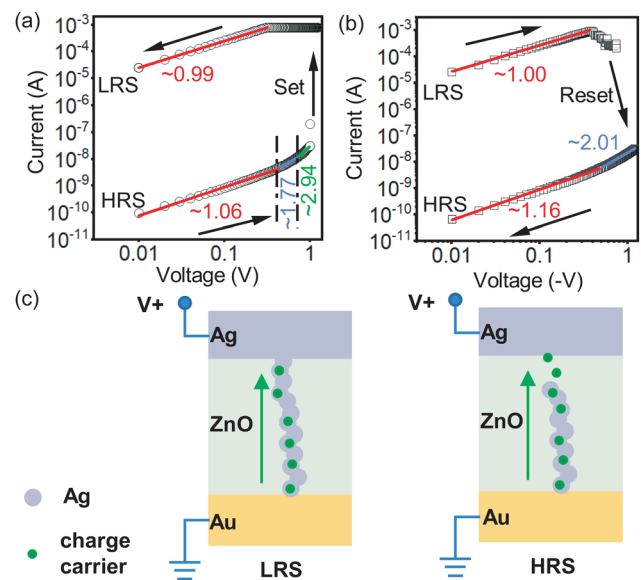


FIG. 5. The I - V characteristic curves of set (a) and reset (b) processes are, respectively, plotted on a double logarithmic scale to investigate the conduction mechanisms under different electrical fields. The arrows in figures are utilized to indicate the direction of voltage sweeping. (c) Illustration of the conducting mechanism of the LRS (left side) and of the HRS (right side). The green arrows indicate the migrating direction of charge carriers.

traps in the active layer, resulting in an exponential increase in the current with a slope of 2.94, which means a transition of trap-unfilled to trap-filled SCLC. The I - V relationships of the HRS conform to the three stages of SCLC, which is summarized in Ref. 33. For the HRS in the reset process [see Fig. 5(b)], an absence of trap-filled SCLC attributes to the abrupt rupture of the conductive filaments, which does not leave enough time for electrons to fully fill up the traps. The different conduction mechanisms of the LRS and the HRS support the formation and rupture of conductive filaments in ZnO to achieve the resistive switching of the inkjet-printed memristor studied in this work.

In summary, by means of inkjet printing, a bipolar resistive switching device, consisting of a Ag/ZnO/Au material stack, can be fabricated and exhibits excellent memory performance such as a low operation voltage of about 0.7 V, a high on/off ratio of 10^7 , a long retention time exceeding 10^4 seconds, and reliable resistive switching over 50 cycles. The conductive mechanisms were studied, and the low resistive state (LRS) is governed by Ohmic conduction, whereas the high resistive state (HRS) is determined by space charge limited conduction.

This work was funded by the Deutsche Forschungsgemeinschaft (DFG, German Research Foundation) under Germany's Excellent Strategy-2082/1-390761711 (Excellent Cluster "3D Matter Made to Order"). Hongrong Hu thanks the Carl Zeiss Foundation for the financial support. We thank Karlsruhe Nano Micro Facility (KNMF), a Helmholtz Research Infrastructure at Karlsruhe Institute of Technology (KIT) for support and access to FIB facilities.

DATA AVAILABILITY

The data that support the findings of this study are available from the corresponding author upon reasonable request.

REFERENCES

- ¹L. Chua, "Memristor-the missing circuit element," *IEEE Trans. Circuit Theory* **18**, 507–519 (1971).
- ²L. O. Chua and S. M. Kang, "Memristive devices and systems," *Proc. IEEE* **64**, 209–223 (1976).
- ³L. Chua, "If it's pinched it's a memristor," *Semicond. Sci. Technol.* **29**, 104001 (2014).
- ⁴D. B. Strukov, G. S. Snider, D. R. Stewart, and R. S. Williams, "The missing memristor found," *Nature* **453**, 80–83 (2008).
- ⁵A. Beck, J. Bednorz, C. Gerber, C. Rossel, and D. Widmer, "Reproducible switching effect in thin oxide films for memory applications," *Appl. Phys. Lett.* **77**, 139–141 (2000).
- ⁶C. H. Kim, Y.-H. Jang, H. Hwang, C. Song, Y. Yang, and J. Cho, "Bistable resistance memory switching effect in amorphous InGaZnO thin films," *Appl. Phys. Lett.* **97**, 062109 (2010).
- ⁷E. Linn, R. Rosezin, S. Tappertzshofen, U. Böttger, and R. Waser, "Beyond von Neumann—logic operations in passive crossbar arrays alongside memory operations," *Nanotechnology* **23**, 305205 (2012).
- ⁸A. Thomas, "Memristor-based neural networks," *J. Phys. D* **46**, 093001 (2013).
- ⁹X. Sheng, C. E. Graves, S. Kumar, X. Li, B. Buchanan, L. Zheng, S. Lam, C. Li, and J. P. Strachan, "Low-conductance and multilevel CMOS-integrated nanoscale oxide memristors," *Adv. Electron. Mater.* **5**, 1800876 (2019).
- ¹⁰E. Gale, R. Mayne, A. Adamatzky, and B. de Lacy Costello, "Drop-coated titanium dioxide memristors," *Mater. Chem. Phys.* **143**, 524–529 (2014).
- ¹¹S. Jung, J. Kong, S. Song, K. Lee, T. Lee, H. Hwang, and S. Jeon, "Flexible resistive random access memory using solution-processed TiO_x with Al top electrode on Ag layer-inserted indium-zinc-tin-oxide-coated polyethersulfone substrate," *Appl. Phys. Lett.* **99**, 142110 (2011).
- ¹²I. Kim, M. Siddik, J. Shin, K. P. Biju, S. Jung, and H. Hwang, "Low temperature solution-processed graphene oxide/Pr_{0.7}Ca_{0.3}MnO₃ based resistive-memory device," *Appl. Phys. Lett.* **99**, 042101 (2011).
- ¹³Y. Lu, S. Gao, F. Li, Y. Zhou, Z. Xie, H. Yang, W. Xue, B. Hu, X. Zhu, J. Shang *et al.*, "Stretchable and twistable resistive switching memory with information storage and computing functionalities," *Adv. Mater. Technol.* **6**, 2000810 (2021).
- ¹⁴X. Feng, Y. Li, L. Wang, S. Chen, Z. G. Yu, W. C. Tan, N. Macadam, G. Hu, L. Huang, L. Chen *et al.*, "A fully printed flexible MoS₂ memristive artificial synapse with femtojoule switching energy," *Adv. Electron. Mater.* **5**, 1900740 (2019).
- ¹⁵M. Nelo, M. Sloma, J. Kelloniemi, J. Puustinen, T. Saikkonen, J. Juuti, J. Häkkinen, M. Jakubowska, and H. Jantunen, "Inkjet-printed memristor: Printing process development," *Jpn. J. Appl. Phys., Part 1* **52**, 05DB21 (2013).
- ¹⁶S. Porro and C. Ricciardi, "Memristive behaviour in inkjet printed graphene oxide thin layers," *RSC Adv.* **5**, 68565–68570 (2015).
- ¹⁷F. M. Simanjuntak, D. Panda, K.-H. Wei, and T.-Y. Tseng, "Status and prospects of ZnO-based resistive switching memory devices," *Nanoscale Res. Lett.* **11**, 368 (2016).
- ¹⁸M. Laurenti, S. Porro, C. F. Pirri, C. Ricciardi, and A. Chiolerio, "Zinc oxide thin films for memristive devices: A review," *Crit. Rev. Solid State Mater. Sci.* **42**, 153–172 (2017).
- ¹⁹M. A. Borysiewicz, "Zno as a functional material, a review," *Crystals* **9**, 505 (2019).
- ²⁰G. Cadilha Marques, D. Weller, A. T. Erozan, X. Feng, M. Tahoori, and J. Aghassi-Hagmann, "Progress report on "from printed electrolyte-gated metal-oxide devices to circuits,"" *Adv. Mater.* **31**, 1806483 (2019).
- ²¹H. Abbas, A. Ali, J. Jung, Q. Hu, M. R. Park, H. H. Lee, T.-S. Yoon, and C. J. Kang, "Reversible transition of volatile to non-volatile resistive switching and compliance current-dependent multistate switching in IGZO/MnO RRAM devices," *Appl. Phys. Lett.* **114**, 093503 (2019).
- ²²H. Wan, P. Zhou, L. Ye, Y. Lin, T. Tang, H. Wu, and M. Chi, "*In situ* observation of compliance-current overshoot and its effect on resistive switching," *IEEE Electron Device Lett.* **31**, 246–248 (2010).
- ²³Z. Zhang, Z. Wang, T. Shi, C. Bi, F. Rao, Y. Cai, Q. Liu, H. Wu, and P. Zhou, "Memory materials and devices: From concept to application," *InfoMat* **2**, 261–290 (2020).
- ²⁴E. Carlos, R. Branquinho, R. Martins, A. Kiazadeh, and E. Fortunato, "Recent progress in solution-based metal oxide resistive switching devices," *Adv. Mater.* **33**, 2004328 (2021).
- ²⁵J. Zhang, H. Yang, Q.-L. Zhang, S. Dong, and J. Luo, "Bipolar resistive switching characteristics of low temperature grown ZnO thin films by plasma-enhanced atomic layer deposition," *Appl. Phys. Lett.* **102**, 012113 (2013).
- ²⁶S. Ali, J. Bae, and C. H. Lee, "Printed non-volatile resistive switches based on zinc stannate (ZnSnO₃)," *Curr. Appl. Phys.* **16**, 757–762 (2016).
- ²⁷G. Vescio, A. Crespo-Yepes, D. Alonso, S. Claramunt, M. Porti, R. Rodriguez, A. Cornet, A. Cirera, M. Nafria, and X. Aymerich, "Inkjet printed HfO₂-based ReRAMs: First demonstration and performance characterization," *IEEE Electron Device Lett.* **38**, 457–460 (2017).
- ²⁸M. N. Awais, H. C. Kim, Y. H. Doh, and K. H. Choi, "ZrO₂ flexible printed resistive (memristive) switch through electrohydrodynamic printing process," *Thin Solid Films* **536**, 308–312 (2013).
- ²⁹S. Zou, P. Xu, and M. Hamilton, "Resistive switching characteristics in printed Cu/CuO/(AgO)/Ag memristors," *Electron. Lett.* **49**, 829–830 (2013).
- ³⁰F.-C. Chiu, "A review on conduction mechanisms in dielectric films," *Adv. Mater. Sci. Eng.* **2014**, 578168.
- ³¹Y. C. Yang, F. Pan, Q. Liu, M. Liu, and F. Zeng, "Fully room-temperature-fabricated nonvolatile resistive memory for ultrafast and high-density memory application," *Nano Lett.* **9**, 1636–1643 (2009).
- ³²M. M. Rehman, G. U. Siddiqui, J. Z. Gul, S.-W. Kim, J. H. Lim, and K. H. Choi, "Resistive switching in all-printed, flexible and hybrid MoS₂-PVA nanocomposite based memristive device fabricated by reverse offset," *Sci. Rep.* **6**, 36195 (2016).
- ³³J. Zhu, T. Zhang, Y. Yang, and R. Huang, "A comprehensive review on emerging artificial neuromorphic devices," *Appl. Phys. Rev.* **7**, 011312 (2020).